Am J Physiol Renal Physiol 300: F721–F733, 2011.
First published December 1, 2010; doi:10.1152/ajprenal.00546.2010.

Impaired endothelial proliferation and mesenchymal transition contribute to vascular rarefaction following acute kidney injury

David P. Basile,[1] Jessica L. Friedrich,[1] Jasmina Spahic,[1] Nicole Knipe,[2] Henry Mang,[2] Ellen C. Leonard,[1] Saeed Changizi-Ashtiyani,[1] Robert L. Bacallao,[2] Bruce A. Molitoris,[2] and Timothy A. Sutton[2]

Departments of [1]Cellular and Integrative Physiology and [2]Medicine, Division of Nephrology, Indiana Center for Biological Microscopy, Indiana University, Indianapolis, Indiana

Submitted 15 September 2010; accepted in final form 28 November 2010

Basile DP, Friedrich JL, Spahic J, Knipe N, Mang H, Leonard EC, Changizi-Ashtiyani S, Bacallao RL, Molitoris BA, Sutton TA. Impaired endothelial proliferation and mesenchymal transition contribute to vascular rarefaction following acute kidney injury. *Am J Physiol Renal Physiol* 300: F721–F733, 2011. First published December 1, 2010; doi:10.1152/ajprenal.00546.2010.—Acute kidney injury induces the loss of renal microvessels, but the fate of endothelial cells and the mechanism of potential vascular endothelial growth factor (VEGF)-mediated protection is unknown. Cumulative cell proliferation was analyzed in the kidney of Sprague-Dawley rats following ischemia-reperfusion (I/R) injury by repetitive administration of BrdU (twice daily) and colocalization in endothelial cells with CD31 or cablin. Proliferating endothelial cells were undetectable for up to 2 days following I/R and accounted for only ~1% of BrdU-positive cells after 7 days. VEGF-121 preserved vascular loss following I/R but did not affect proliferation of endothelial, perivascular cells or tubular cells. Endothelial mesenchymal transition states were identified by localizing endothelial markers (CD31, cablin, or infused tomato lectin) with the fibroblast marker S100A4. Such structures were prominent within 6 h and sustained for at least 7 days following I/R. A Tie-2-cre transgenic crossed with a yellow fluorescent protein (YFP) reporter mouse was used to trace the fate of endothelial cells and demonstrated interstititial expansion of YFP-positive cells colocalizing with S100A4 and smooth muscle actin following I/R. The interstitial expansion of YFP cells was attenuated by VEGF-121. Multiphoton imaging of transgenic mice revealed the alteration of YFP-positive vascular cells associated with blood vessels characterized by limited perfusion in vivo. Taken together, these data indicate that vascular dropout post-AKI results from endothelial phenotypic transition combined with an impaired regenerative capacity, which may contribute to progressive chronic kidney disease.

capillary; fibroblast; fibrosis

ACUTE KIDNEY INJURY (AKI) remains a significant clinical problem with increasing incidence and high mortality rates (10, 43). In surviving patients, recovery of renal function is generally expected. However, several studies suggested that a significant population of patients with AKI develops a predisposition toward chronic kidney disease (CKD) (1, 11, 14). Moreover, delayed graft function following kidney transplantation is strongly associated with subsequent loss-of-graft function following initial recovery (29). These observations suggest a causal link between acute kidney injury on long-term kidney function and CKD progression.

Rodent models of AKI using ischemia-reperfusion (I/R) have been utilized to study the injury process as well as subsequent repair and recovery processes. In addition to reductions in glomerular filtration rate, severe I/R injury results in proximal tubular damage and cell death via necrosis or apoptosis (32). Proliferation of epithelial cells represents an important component of the recovery and regenerative responses (28). In animal models, recovery can be enhanced by exogenous addition of epithelial mitogens such as EGF, HGF, or IGF-I that increase epithelial proliferation, whereas impaired proliferation in aging is associated with impaired recovery (27, 35).

The renal vasculature is also injured in response to I/R injury. In contrast to proximal tubules, the renal vasculature lacks efficient regenerative capacity leading to a persistent 30–50% reduction in vascular density following I/R (4, 12). Reductions in vascular density have also been reported in other rodent models of kidney injury induced by folate (45), ureteral obstruction (9), or in response to inhibition of nitric oxide synthase (NOS) (30). The reduction in vascular density may have important functional consequences by promoting hypoxia and by impairing hemodynamic and sodium regulatory responses to predispose chronic kidney disease and hypertension (2, 3, 17, 33).

The mechanism for vascular loss during AKI relates in part to the presence or absence of humoral trophic cues (2, 5). Immunoneutralization of TGF-β, which is expressed transiently following experimental AKI, was shown to preserve renal vascular structure and reduced the number of tubulointerstital fibroblasts present after 5 wk of recovery (38). In addition, vascular endothelial growth factor (VEGF) expression is transiently reduced following experimental AKI; administration of a nonheparin-binding form of VEGF (VEGF-121) protected rats from vascular dropout and mitigated long-term functional anomalies (19). Interestingly, protection was conveyed by VEGF when administered during the early remodeling period, but the delayed administration of VEGF (i.e., 3 wk post-I/R) did not provide any long-term functional protection from I/R (19).

The current understanding of the cellular events involved in vascular remodeling and how VEGF may impinge on such events following AKI remains unclear. VEGF administration may preserve vascular structure by ameliorating early endothelial cell damage and/or promoting a vascular regenerative response in part via proliferation. However, there have been no studies specifically addressing the endothelial proliferative response of AKI with or without the influence of endothelial mitogens. Although there is evidence of endothelial injury based on morphological and endothelial barrier studies, evidence demonstrating I/R-induced endothelial cell death is scant. A recent study, Horbelt et al. (12) demonstrated a

Address for reprint requests and other correspondence: D. P. Basile, Dept. of Cellular and Integrative Physiology, Indiana Univ. School of Medicine, 635 Barnhill Dr. MS 334, Indianapolis, IN 46202 (e-mail: dpbasile@iupui.edu).

modest expression of activated caspase-3 but could not identify endothelial apoptosis by TUNEL in Tie-2/GFP mouse kidney following I/R injury. An alternative explanation for endothelial cell loss is the possible phenotypic transition to a mesechymal/fibroblastic phenotype. Endothelial mesenchymal transition (endoMT) could explain not only the resultant loss of renal microvessels, but also the deposition of tubulointerstial fibroblasts that are evident following recovery from I/R injury. Therefore, the purpose of this study was to evaluate the hypothesis that vascular loss following AKI results from an impaired endothelial proliferative response and/or phenotypic transition and that VEGF-121 may modulate either one or both of these processes.

METHODS

Animals. Care of the rats before and during the experimental procedures was conducted in accordance with the policies of the National Institutes of Health (NIH) *Guide for the Care and Use of Laboratory Animals*. All protocols had received prior approval by the Institutional Animal Care and Use Committees at Indiana University.

Male Sprague-Dawley rats ~250 g were obtained from Harlan (Indianapolis, IN) and housed in pairs in standard shoe-box cages. Homozygous B6.129X1-Gt(ROSA) 26Sor$^{tm1(EYFP)Cos}$/ J female mice (Jackson Laboratory stock no. 006148) were mated with hemizygous male Cg-Tg(Tek-cre)12Flv/J (Jackson Laboratory stock no. 004128). Cre-positive offspring used in the studies were identified from tail DNA by the use of standard PCR procedures and the Cre primer sequences (5′-GCGGTCTGGCAGTAAAAACTATC-3′ and 5′-GTGAAACAGCATTGCTGTCACTT-3′, yielding an amplicon of ~100 bp).

Mice and resulting pups were housed in standard shoe-box sized cages on a 12:12-h light-dark cycle. Animals were housed with a 12:12-h light-dark cycle and provided standard laboratory chow (Teklad, Harlan) and water available ad libitum.

Surgeries and treatments. AKI in rats was carried out as described previously (19). Rats were anesthetized with ketamine (100 mg/kg ip) and pentobarbital sodium (25 mg/kg ip) and placed on a heated surgical table. After a midline incision, microvascular clamps were placed on the renal pedicles of both kidneys. After 35 min, the clamps were released and reperfusion was visualized. Sham-operated groups were exposed to the same treatments except that the kidneys were not touched.

AKI in mice was carried out as described previously (12). Anesthesia was induced with 5% isofluorane and then maintained at 1.5% isoflurane. Mice were placed on a heated surgical pad. After a midline incision, microvascular clamps were placed on the renal pedicle for 18 min and then released.

VEGF-121 was a generous gift from Scios (Mountain View, CA) and was diluted in 0.9% NaCl as a vehicle. In some studies, VEGF-121 was administered to rats or mice at a dose of 100 $\mu g \cdot kg^{-1} \cdot day^{-1}$ sc, in two daily injections, with the first administration beginning at the time of reperfusion. In some studies (see RESULTS), BrdU was diluted in 0.9% NaCl and administered twice daily for up to 7 days at a dose of 120 mg/kg.

For measurement of renal function, tail blood samples were collected into heparanized tubules. For rats, serum creatinine values were

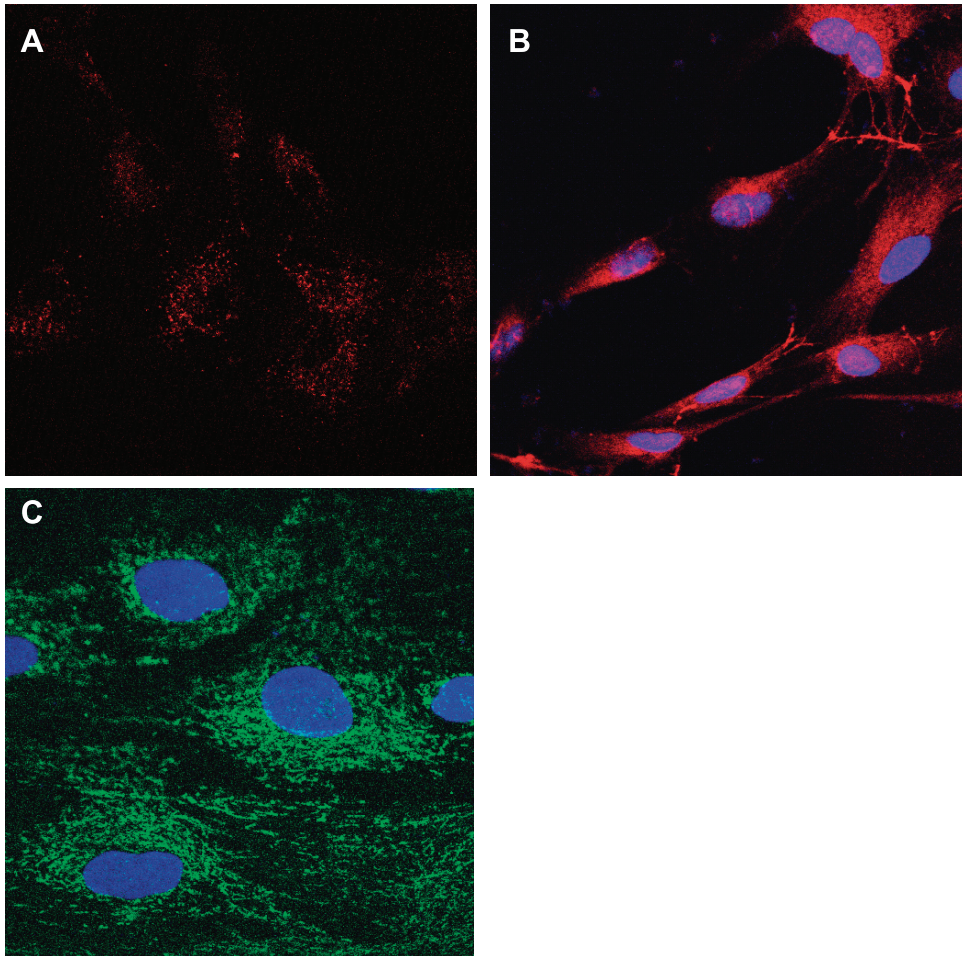

Fig. 1. Cablin antibody-mediated cell sorting in rat kidney. Rat kidney tissue was minced, collagenase digested, and subjected to FACS using an antibody generated against cablin. Cablin +-sorted cells were then plated and cultured for 2 days and endothelial phenotype was evaluated by visualizing acetylated LDL uptake (*A*), von Willebrand factor staining (*B*), and expression of CD31/PECAM staining (*C*). Samples in *B* and *C* were counterstained with DAPI.

determined using a Creatinine II analyzer (Beckman Coulter), while measurement of serum creatinine in mice was carried out via capillary electrophoresis (O'Brien Kidney Disease Center, University of Texas Southwestern Medical School). The resultant injuries were consistent with those from previous studies (19) and VEGF administration did not influence creatinine values with respect to vehicle-treated controls.

At termination of the study, animals were deeply anesthetized with ketamine (50–100 mg/kg ip) and pentabarbitol sodium (25 mg/kg ip) as needed. Kidneys were harvested and frozen or fixed for immunohistochemical procedures as described in greater detail below. In some studies, functional vessels were identified by intravenous administration (5 min before euthanasia) of biotinylated-lycopersicon esculentum lectin (1.25 mg/kg tomato lectin; Vector Laboratories), which labels endothelial cells only in perfused vessels (42).

Endothelial cell culture. Kidneys were removed quickly from Sprague-Dawley rats and placed in 4–5 ml of α-MEM with 5% fetal bovine serum (Sigma, St. Louis, MO, serum from Hyclone, Logan, UT). After being minced with a scalpel, the tissue was incubated with 1 mg/ml collagenase/dispase solution (Roche, Indianapolis, IN) at 37°C for 45–60 min, with pipetting every 10 min to aid in digestion. After centrifugation, residual red blood cells were lysed (Red Blood Cell Lysis Buffer, Sigma), and cells were filtered through a 70-μm cell strainer (Fisher, Pittsburgh, PA). After the sample was blocked (Fc block, 1 μg/million cells; PharMingen, Bedford, MA), the cells were stained with rabbit anti-cablin and an FITC-labeled goat anti-rabbit secondary antibody. Following staining, cells were resuspended in α-MEM with 15% FBS, 5 ng/ml vascular endothelial growth factor (Sigma), 50 ng/ml basic-fibroblast growth factor (Sigma), and 50 μg/ml endothelial cell growth supplement and filtered twice through a 40-μm cell strainer (Fisher). Cells were then sorted at 1×10^6 cells/ml using FACS Vantage sorter (Bio-Rad, Hercules, CA). The resultant positive cells were cultured for 2 days before characterization.

Immunohistochemistry. Primary antibodies used in these studies were as follows: the rabbit anti-cablin antibody utilized in this study was described previously (8). The rabbit anti-CD31/PECAM (SEW31) antibody was generous gift of Dr. P. Newman (Blood Center of Southeast Wisconsin). The rabbit anti-S100A4/FSP-1 was obtained from Dako (#A511401); mouse anti-BrdU was directly conjugated to Alexa fluor 488 and obtained from Invitrogen; mouse anti-yellow fluorescent protein (YFP) was obtained from Abcam (no. ab290); mouse α-SMA was obtained from (Invitrogen no. 18–0106).

For light microscopy studies to detect tomato lectin binding, formalin-fixed, paraffin-embedded sections were dewaxed and rehydrated in xylene and decreasing concentration of EtOH according to standard techniques. Slides were incubated with streptavidin-conjugated alkaline phosphatase and developed with nitroblue tetrazolium (Vector Blue, Vector Laboratories). Following washing and subsequent avidin and biotin blocking steps (Zymed), the S100A4/FSP-1 was detected using the red-colored AEC as the substrate (Zymed), according to our previous approach (37).

Immunofluorescent studies were carried out in tissues that were immersion fixed in 100% ice-cold methanol and sectioned at ~100 μm using a vibratome. For immunofluorescent analysis of the endothelial-specific markers CD31 or cablin, specific methodologies were developed, since both of these primary antibodies derive from rabbit. First endogenous peroxidases in free-floating sections were inhibited by treatment with 2.1% H_2O_2 for 45 min followed by 30-min incubation in blocking solution consisting of 0.1 M Tris, pH 7.5, containing 0.9% NaCl, 0.5% BSA (USB), 0.05% fish skin gelatin (Sigma), and 0.1% Triton X-100 (Sigma). The first antibody in the sequence was incubated for ~18 h at 4°C with gentle agitation at a concentration of 1:200,000 dilution or 0.0624 μg/ml, respectively, for

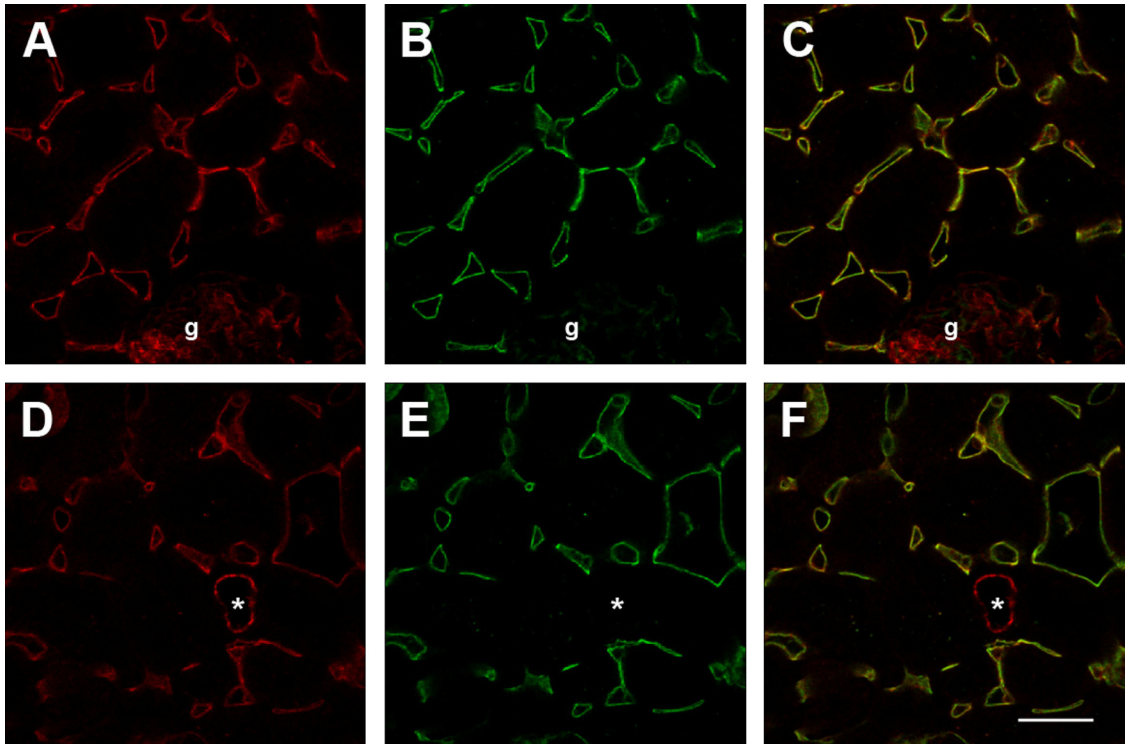

Fig. 2. Cablin/PECAM staining of peritubular capillaries of rat kidney. Methanol-fixed rat kidney tissues were subjected to immunofluorescent double labeling using tyramide enhancement as described in METHODS. Shown are representative confocal images of Cy-3-labeled cablin (*A*, *D* shown in red), FITC-labeled PECAM/CD31 (*B*, *E*, shown in green). The merged images shown in *C* and *F* reveal extensive colocalization in peritubular vessels. Note in images *A–C*, from renal cortex, that the glomerulus (indicated by g) is largely PECAM+/cablin-, while the arteriole in *D* and *E* (indicated by *) is also PECAM+/cablin negative. The experiment was done with dye reversal and yielded similar results (not shown); bar in *D* = 25 μm.

either anti-cablin or anti-CD31. The tissues were rinsed extensively for up to 3 h at room temperature in blocking solution with at least three changes. Tissues were then incubated for up to ~18 h in goat anti-rabbit-HRP (1:10,000 Southern Biotech no. 4030–05). Following rinsing, the signal was developed using a tyramide Cy3 amplification kit according to the manufacturer's instructions (Perkin Elmer no. NEL744001KT). The second antibody in the sequence was then incubated for 18 h at a higher concentration (1:1,000 for cablin, and 1:500 for PECAM), which could be detected directly by subsequent incubation with FITC-conjugated goat anti-rabbit IgG (Zymed #65–6111). Control experiments demonstrated the concentration of primary antibodies that were detected using tyramide amplification in the initial part of this procedure is too low to be detected by the FITC-conjugated anti-rabbit IgG antibodies that are used to detect the second of the primary antibodies in the sequence. Following a final rinsing, tissues were mounted on slides and coverslipped in a solution of 50% glycerol/20% Mowiol (Calbiochem) and allowed to dry overnight.

The approach described above was modified for other double-staining protocols. For double-labeling of endothelial cells and fibroblasts, CD31 or PECAM was initially developed using tyramide amplification (Cy3 or fluorescein; Perkin Elmer) and subsequent labeling of fibroblasts was carried out by incubating tissues in anti-S100A4 (1:50) followed by goat anti-rabbit IgG conjugated to either FITC or Cy3.

For analysis of BrdU-positive endothelial cells, methanol-fixed vibratome sections (~100 μm) were incubated in 2 N HCl at 37°C for 1 h and then neutralized in borate buffer, pH 8.4, for 20 min with subsequent PBS washes. Sections were then blocked and placed in anti-BrdU conjugated with AlexaFluor 488 (Invitrogen #A21303). After being rinsed, endothelial cells were detected using anti-cablin and tyramide-Cy3 development as described above.

For staining of yellow fluorescent protein, tissues were fixed in 2% paraformaldehyde for 1 h, transferred into PBS, and stored 4°C until use. YFP protein was detected in 100-μm-thick vibratome sections using rabbit anti-GFP (1:200,000) and developed using Cy3 tyramide amplication, as described above. In some tissues, costaining was carried out for S100A4 as described above. In other studies, tissues were incubated with mouse anti α-SMA (1:50) after IgG blocking (M.O.M. Vector kit, Vector Laboratories FMK-2201). Following being washed, tissues were incubated overnight in anti-IgG2a conjugated with Alexa Fluor 488 secondary antibody (Invitrogen #A21131). As a negative control, a mouse IgG2a isotype (Invitrogen #MG2a00) was used in place of the primary antibody.

Microscopy and tissue analysis. Tissues were visualized for light microscopy using a Nikon Optiphot-2 upright microscope equipped with a Spot digital camera and image acquisition software (version 3.4.5; Diagnostic Instruments). For quantitative analysis, five random images through renal cortex and outer medulla ~0.24 mm^2 were obtained and used to manually count S100A4/FSP-1-positive cells. Data are expressed as S100A4-positive cells per field.

For fluorescence detection, images were obtained using a Zeiss LSM NLO confocal microscope equipped with Ar and HeNe lasers. Images were obtained using a ×40 water immersion lens. For fluorescein, excitation was at 488 and detection from 500–530 nm, while Cy3 was detected by excitation at 545 and detection at 565–615.

For quantification of BrdU-labeled cells, eight images in cortex and outer medulla were obtained using the standard 1×-zoom setting corresponding to an area of 0.053 mm^2; BrdU-positive cells were counted from images manually and expressed as number of positive cells per field. For discrimination of colocalized vs. adjacent structures, four nonoverlapping images were from each field were obtained using 2× zoom setting. For quantification of vascular density, CD31-stained structures overlying an arbitrary 12 × 12 grid were counted from 4–5 random images from cortex and from outer medulla as described previously (19); data are expressed as percent of sham-operated control. For quantification of YFP immunohistochemistry, five random images with a area 0.053 mm^2 were obtained; images acquired in the 565–615 range were analyzed for surface area with the aid of NIH image J software and data were expressed as percent surface area.

For live multiphoton microscopy, the left kidney of the pentobarbital sodium-anesthetized mouse was imaged through a retroperitoneal window via a left flank incision using an Olympus FV1000-MPE confocal/multiphoton microscope (Center Valley, PA) equipped with a MaiTai Deep See tunable laser (Spectra Physics/Newport, Santa Clara, CA) mounted on an Olympus IX81 inverted microscope stand. Two hundred microliters of rhodamine-conjugated dextran (500,000 mol wt, 3.25 mg/ml in 0.9% saline) were injected via the tail vein of the anesthetized mice at the time of imaging. Image processing was performed utilizing MetaMorph software (Molecular Devices, Silicon Valley, CA).

RESULTS

Effective labeling of renal endothelial cells using anti-CD31 and anti-cablin antibodies. To effectively examine endothelial dynamics, we first verified the specificity of the anti-cablin antibodies used previously to stain renal peritubular blood vessels (8, 19). Collagenase-dispersed rat kidney cells were subjected to FACS sorting using anti-cablin and the collected cells were placed in culture for a period of 2 days. The resulting cultured cells incorporated acetylated-LDL, and expressed von Willebrand factor and CD31/ PECAM, characteristic of endothelial cells (Fig. 1). A double-staining method was developed to compare the localization of cablin with CD31/PECAM. CD31/PECAM was detected using tyramide amplification of Cy3 followed by localization of cablin and visualization with an FITC-labeled secondary antibody. CD31 staining was evident in peritubular capillaries of normal rat kidney following tyramide amplification with Cy3 and was also present in capillaries of the glomerulus (g) and small

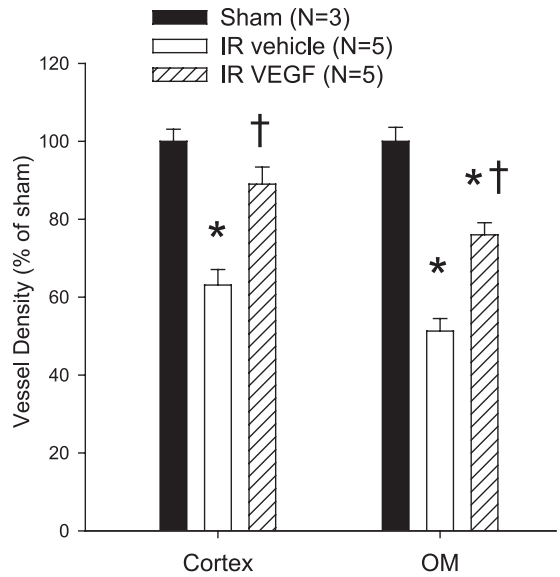

Fig. 3. Effect of acute kidney injury (AKI) and vascular endothelial growth factor (VEGF)-121 on renal vascular density following 7 days of recovery from renal ischemia-reperfusion (I/R). Shown are data from morphometric analysis of cablin immunofluorescence-stained microvessel structures intersecting arbitrary grid lines and expressed as a percentage sham-operated control group; $n = 5$ animals per group. *$P < 0.05$ vs. sham-operated control. †$P < 0.05$ VEGF-121-treated vs. vehicle-treated group by ANOVA and Student-Newman-Keuls post hoc test.

arterioles (*; Fig. 2, *A* and *D*). Anti-cablin antibodies labeled the same peritubular capillaries but did not prominently label capillaries of the glomerulus or small arterioles (Fig. 2, *B* and *E*). The merged images (Fig. 2, *C* and *F*) indicate a significant overlap of the two signals. Taken together, these data indicate that cablin antibody is highly preferential to labeling renal endothelial cells in the peritubular microvasculature.

Effects of VEGF-121 on BrdU incorporation post-I/R injury. The specificity of anti-cablin was utilized to evaluate the effect of VEGF-121 on endothelial cell proliferation during the recovery phase of AKI. Rats were subjected to 35 min of I/R injury and net cumulative cell proliferation was evaluated by repetitive administration of BrdU twice daily during the recovery periods ranging from 1, 2, or 7 days following I/R. The effect of I/R and VEGF-121 on vascular density was evaluated based on the distribution of cablin+ staining; at 7 days post-I/R, there was a significant 37 and 49% reduction in vascular density in the cortex and outer medulla, respectively, relative to sham-operated controls. Similar to results in previous studies (19), VEGF-121 did not affect the peak of the early loss of renal function following I/R relative to vehicle (not shown), but significantly attenuated I/R induced vessel loss (Fig. 3).

The identification of proliferating endothelial cells was facilitated by double labeling of BrdU with CD31-positive structures. Relatively few BrdU (green) cells were identified in confocal sections of sham-operated rat kidney, while BrdU-positive cells were abundant following 7 days of recovery from I/R injury (Fig. 4*A*). BrdU-positive cells were prominent within the tubular epithelium (Fig. 4, white arrows), and a smaller number of BrdU+ cells were observed within the interstitial region comprising both endothelial cells (CD31-positive; blue arrow, Fig. 4, *A′* and *C′*) and nonendothelial cells (CD31-negative; yellow arrow, Fig. 4, *A′*, *B′*, *C′*).

The number of BrdU-positive cells increased at each successive time point and was about twofold greater in the outer medulla vs. the cortex (Fig. 5). After 7 days of recovery with BrdU treatment, 95.4 ± 1.1% of all BrdU-positive cells were apparent within tubules, while 4.5 ± 0.5% of positive cells were in the interstitial perivascular zone (compare Fig. 5, *top*, with Fig. 5, *middle* and *bottom*). Of the BrdU-postive interstitial cells, the majority were nonendothelial, while only a small number (1.0 ± 0.2%) were BrdU+/CD31+ endothelial cells. No BrdU+/CD31+ cells were detected within the first 2 days following recovery from I/R. Despite the protective effects on the vasculature (Fig. 4), VEGF-121 did not influence BrdU incorporation in endothelial, perivascular, or tubular compartments (Fig. 5). These data highlight the limited proliferative capacity of renal endothelial cells following I/R injury and that VEGF-121-mediated protection likely occurs via a nonproliferative mechanism.

Endothelial cells are a source of interstitial fibroblasts following I/R injury. Potential endoMT was identified by localizing the fibroblast marker, FSP1/S100A4, to vascular endothelial cells. Tomato lectin (TL, biotin conjugated) was administered intravenously to sham or post-I/R rats 5 min before tissue harvest. TL decorated renal vessels in both cortex and outer medulla of sham-operated rats (Fig. 6*A*, blue stain). S100A4 cells are shown in red (Fig. 6, *B* and *C*); the number

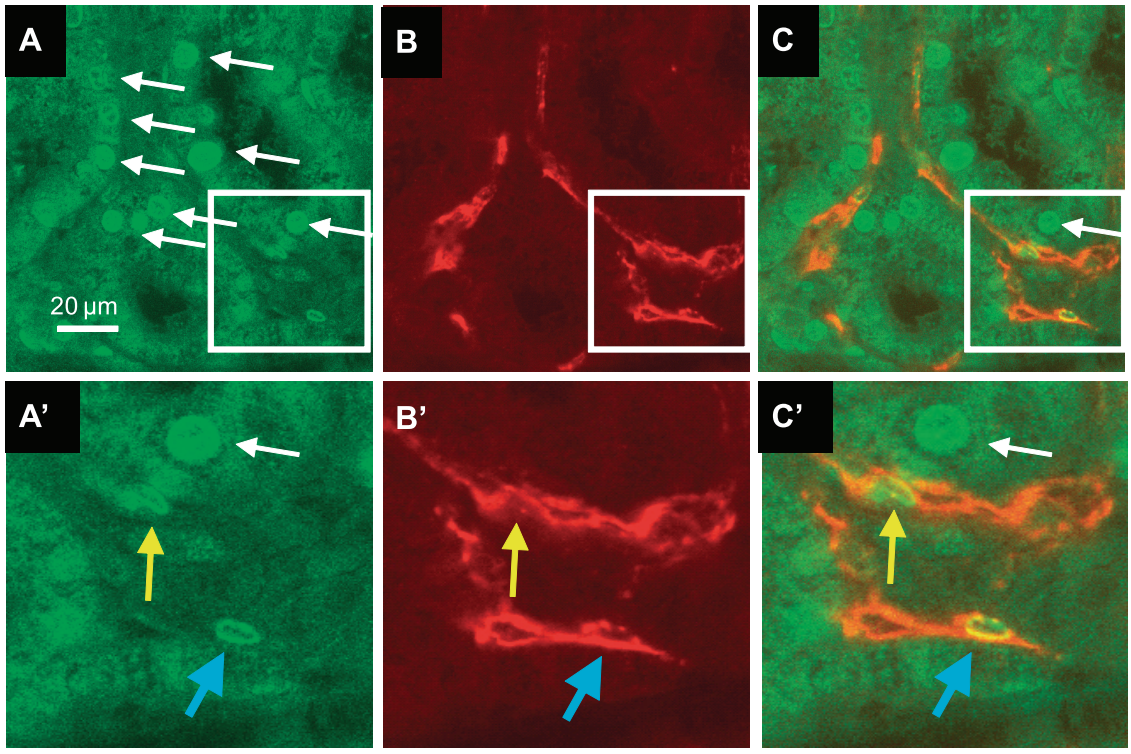

Fig. 4. Identification of proliferating cells in tubular epithelial and vascular endothelial cells following recovery from AKI. Shown are representative confocal images from the kidney of a rat that was given BrdU twice daily for 7 days of recovery from I/R injury. *A*: BrdU-positive cells in the green channel. *B*: cablin+ endothelial cells in the red channel. *C*: merged image. Note the prominent expression of BrdU in tubular epithelial cells. Higher magnification is shown in *A′*, *B′*, and *C′*, which correspond to the *inset*. Blue arrow indicates a cablin+ BrdU+ cell in the interstitial area, while the yellow arrow indicates a cablin-/BrdU+ in the interstitial area. Magnification is shown in *A*.

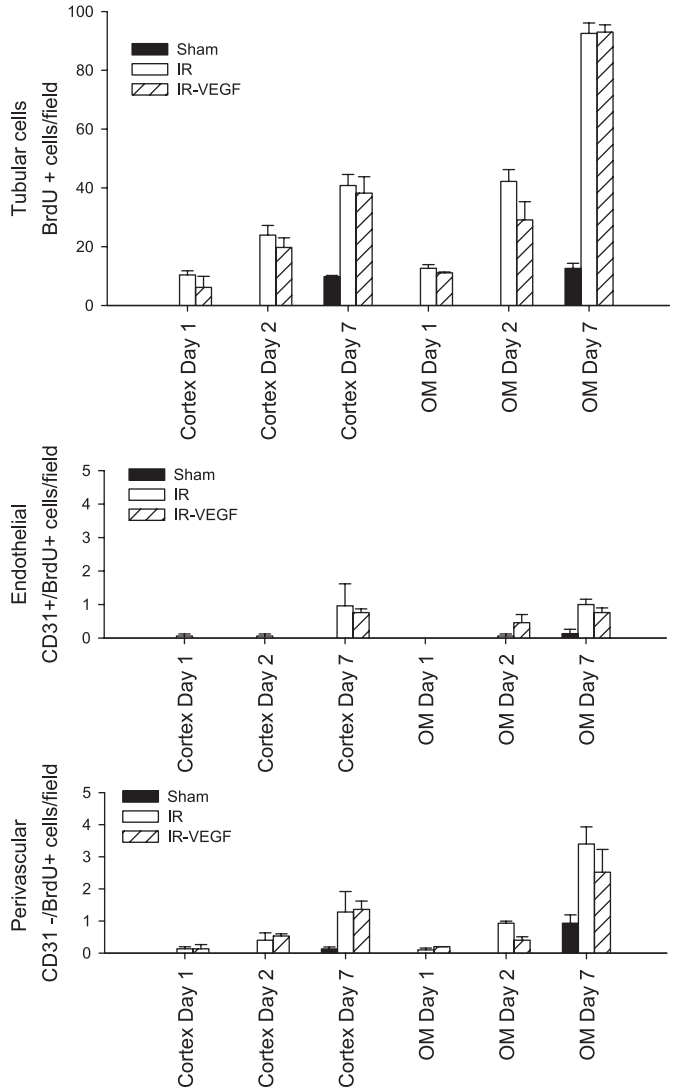

Fig. 5. Lack of effect of VEGF-121 on proliferation during recovery from AKI. The number of BrdU-positive cells are shown based on their distribution in tubular cells (*top*), endothelial cells (*middle*), and perivascular cells (*bottom*). Data are shown for both cortex and outer medulla at 1, 2, and 7 days of recovery for AKI group (open bar, $n = 5$ per each time point) and AKI VEGF-121-treated group (striped bar, $n = 3$). Sham-operated controls (filled bar) was carried out only in the 7-day period. No effect of VEGF-121 was observed on BrdU incorporation in any cellular compartment following I/R injury.

of these cells rose significantly above sham levels within 6 h of I/R and was maintained above sham for at least 7 days (Fig. 6*D*). Discrete S100A4+ labeled cells were apparent in vascular structures stained with TL, indicating potential transition states (Fig. 6*B*, *inset*). For example, at 6 h of reperfusion, a significant number of cells were identified as TL-positive vascular cells (6.4 ± 0.8% in cortex; 5.0 ± 2.1% in outer medulla) while a smaller but sustained level of S100A4 cells were TL positive at later time points (Fig. 6*E*, filled bars). In contrast, potential epithelial tubular transition states were considerably less prevalent; for example, only 0.15% of S100A4 cells were observed in tubular epithelial cells at 6 h of reperfusion (Fig. 6*E*, open bars).

Additional double staining using immunofluorescent histochemistry was also carried out to verify further the presence of potential endoMT transition states using either CD31/PECAM or cablin to label renal endothelial cells in the early postinjury state. Similar to the results observed using TL, S100A4 is not prominent in sham-operated control kidney but readily apparent in the postischemic kidney at 6 h (stained green in Fig. 7*E* and red in Fig. 8*B*). EndoMT transition states were readily identified using both endothelial specific antibodies and regardless of which fluorophore was employed to label endothelium and mesenchymal cell types (CD31-Cy3, Fig. 7; cablin-FITC, Fig. 8).

A mouse model to trace endothelial cell fate was developed by crossing transgenic mice expressing endothelial targeted cre-recombinase (Tie2-Cre) with a floxed YFP reporter mouse to generate mice expressing YFP in endothelial cells and their subsequent progeny. Mice heterozygous for both Cre and YFP were subjected to sham surgery or I/R and recovery for 14 days with or without VEGF-121 administration. YFP-positive staining was evident in peritubular vascular structures of sham-operated control mice (Fig. 9, *B* and *C*). The distribution of YFP-positive staining was enhanced in the tubulointerstitial area after 14 days of recovery from I/R, which was accompanied by hetergeneous colocalization with either S100A4 (Fig. 9, *E* and *F*) or, to a lesser extent, the myofibroblast marker, α-smooth muscle actin (Fig. 9, *M* and *N*). In Cre-negative mice, S100A4 staining was prominent following injury, but no signal was detected by the YFP antibody (Fig. 9*K*). Importantly, the distribution of YFP-positive staining was significantly attenuated in the VEGF-treated animals (Figs. 9, *G–I*, and 10).

Multiphoton imaging was used in sham-operated and post-IR mice to visualize vascular blood flow in Tie-2-Cre/YFP mice in vivo. In sham-operated mice, YFP fluorescence was evident in vascular structures and cortical blood flow was visualized in peritubular vessels using a red fluorescent high-molecular-weight dextran (Fig. 11*A* and supplemental movie; the online version of this article contains supplemental data). In contrast, there were several YFP-expressing cells deposited in the tubulointerstitial areas that completely lacked flow, or in which flow was limiting. The YFP cells in areas with compromised flow showed a different morphology than YFP cells of sham-operated mouse kidneys (arrowheads in Fig. 10*B* vs. thin arrows in Fig. 11*A*, and supplemental movie).

DISCUSSION

It is well-accepted that local growth factors are synthesized in response to AKI and that repair of the renal epithelium is due, in part, to this trophic activity (27, 28). A further increase in epithelial cell proliferation to exogenously administered growth factors demonstrates the highly proliferative nature of these cells during the repair process (13, 25, 27, 28). Renal vascular loss may be due to a lack of appropriate vascular trophic support in response to injury as well as an impaired responsiveness of vascular cells. The impaired vascular response occurs in the presence of hypoxia, which is exacerbated in the kidney immediately and is sustained following AKI due to both renal vasoconstriction and capillary loss, respectively (3). Although hypoxia is typically thought to stimulate the synthesis and release of proangiogenic factors such as VEGF, the expression of VEGF does not increase but rather transiently decreases following AKI (5). Interestingly, other

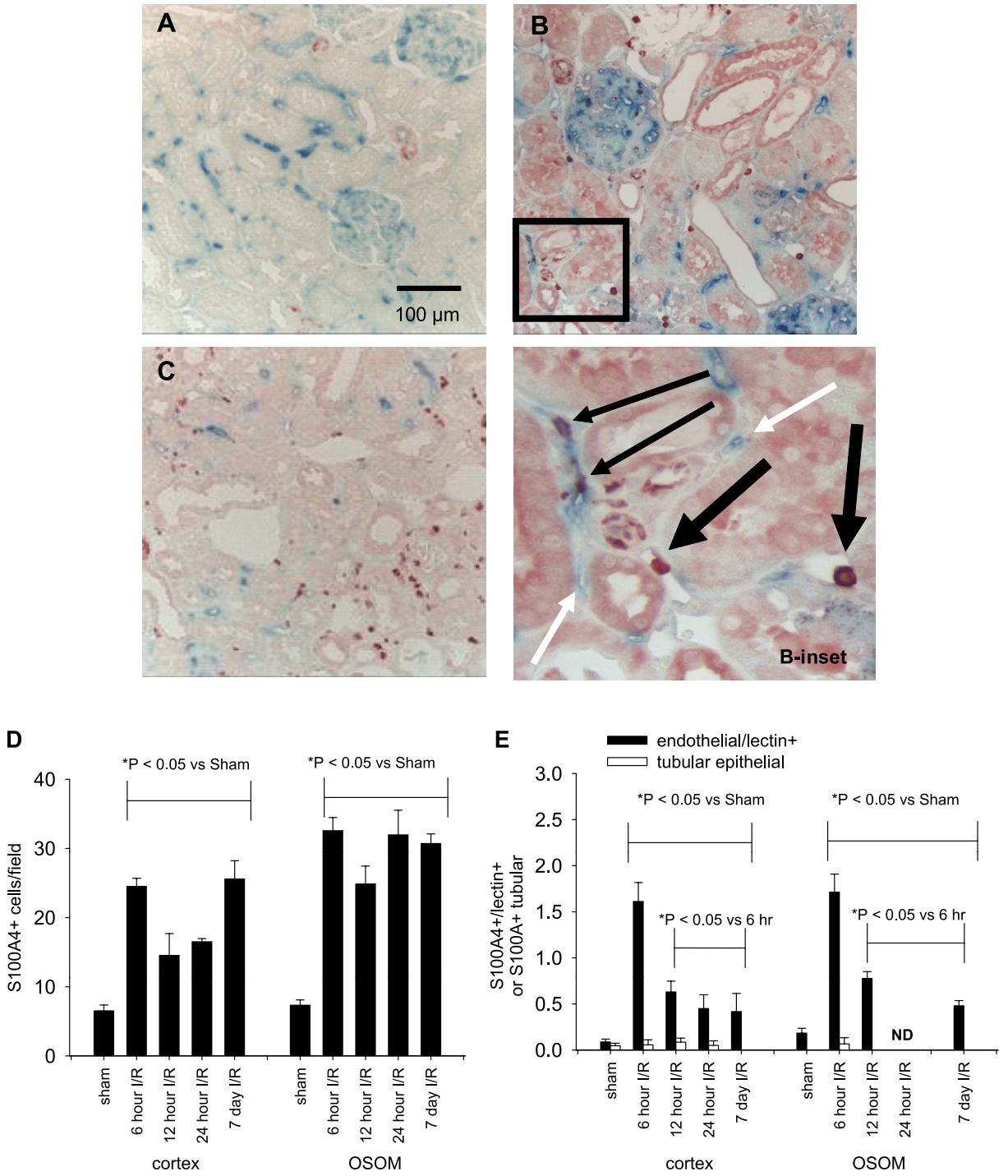

Fig. 6. Colocalization of S100A4/FSP-1 with tomato lectin following renal I/R injury. Biotinylated tomato lectin (TL) binding to vascular endothelial cells is shown in blue, while S100A4/FSP-1 staining is shown in red in kidneys of sham-operated rats (*A*) and rats following recovery from I/R for 6 h (*B*) and 7 days (*C*). *Inset*: higher magnification of the area in *B*, which illustrates colocalization of S100A4 staining in peritubulular vascular structures (indicated by the thin black arrows). Vascular structures without corresponding S100A4/FSP-1 staining (white arrows) were also prominent. Note the presence of S100A4/FSP-1+ in the lumen of venular spaces with a macrophage appearance in the early (6-h post-AKI group, thick dark arrow). Magnification is shown in *A*. Quantification of total number of S100A4/FSP-1+ cells in response to I/R injury is shown in *D* for both cortex and outer medulla. *E*: potential endothelial mesenchymal transition states defined as S100A4+/lectin+ structures (filled bars) and potential epithelial mesenchymal states, defined as S100A4+ cells in tubular cells (open bars). ND indicates that TL was not detectable in the outer stripe of outer medulla (OSOM) at 24 h of reperfusion; $n = 4$ animals per group. $^*P < 0.05$, significant differences as shown based on ANOVA and Student-Newman-Keuls post hoc test.

models of progressive renal disease that are characterized by peritubular capillary dropout (e.g., hypokalemia and aging) manifest both hypoxia and a paradoxical decrease in VEGF expression (18, 34).

Although there is evidence for decreased vascular trophic support in progressing renal interstitial disease, it is important to consider vascular cell responses to both injury and exogenously provided factors such as VEGF with potential thera-

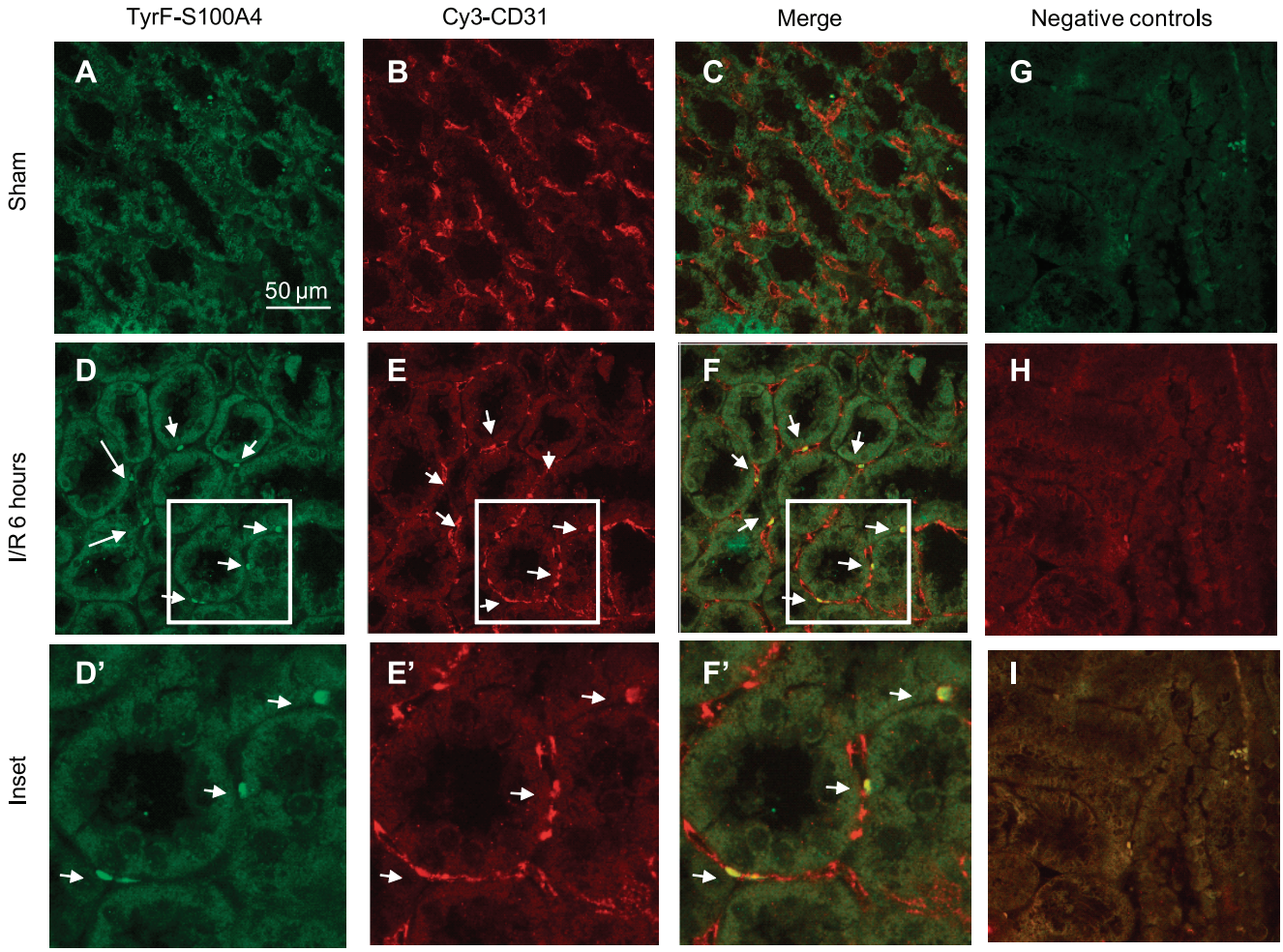

Fig. 7. Colocalization of CD31 and S100A4 by immunofluorescence following I/R injury. Representative confocal images are shown from sham-operated rat kidney (*A–C*) and kidney of rats 6 h following renal I/R injury (*D–I*). S100A4 staining was achieved by tyramide amplification of fluorescein (*A*, *D*), while CD31 staining was visualized directly using Cy3-labeled secondary (*B*, *E*; see METHODS), while merged images are shown in *C* and *F*. Magnification is shown in *A*. *D′*, *E′*, and *F′* are enlarged from the outlined region and indicate cells expressing both S100A4 and CD31 (white arrow). Negative controls resulting from omission of primary antibodies are shown in green, red, and merged settings are shown in *G–I*, respectively. Staining representative of 5 animals per group.

peutic utility. VEGF is a potent endothelial mitogen and stimulates endothelial cell proliferation in vitro and during vascular remodeling in response to hypoxia in cardiac tissue, skeletal muscle, and tumor formation (26, 41). The administration of VEGF-121, a nonheparin-binding form of VEGF, preserves the renal vasculature of rats following AKI and ameliorates secondary complications associated with elevated salt intake (19). In these studies, only groups treated with VEGF-121 early in the injury process were protected from loss of vascular density and subsequent salt-sensitive injury, while delayed treatment did not protect from subsequent salt-sensitive injury. Interestingly, Long et al. (23) used a model of salt-sensitive hypertension induced by a 2-wk administration ANG II; delayed administration of VEGF-121 beginning 1 wk later had beneficial effects on tissue damage but did not restore capillary density, indicating that VEGF protection in kidney may occur independent of de novo vascular repair. Based on these observations, we sought to determine whether VEGF-121 promoted endothelial proliferation in the early stages of I/R injury.

While endothelial proliferation is documented in models of glomerular origin (31), few studies examined proliferative responses of the peritubular vasculature in response to injury. With the goal of maximizing detection of proliferating endothelial cells, repetitive BrdU administration was conducted for up to 7 days. As expected, tubular cells comprised the vast majority of BrdU-positive cells, which steadily increased as renal regeneration proceeded. Although some BrdU-positive perivascular/interstitial cells were identified, most were not endothelial, but rather in close proximity to CD31-positive endothelial cells. While there was considerable tubular proliferation evident in the first 2 days following ischemic AKI, no BrdU-positive endothelial cells were identified within this time frame. Moreover, after 7 days, the number BrdU-positive endothelial cells was less than 1 per microscopic field in post-AKI/VEGF-treated rats, which was not significantly different than sham-operated animals. We suggest this lack of proliferation represents a fundamental basis for the impaired renal vascular regeneration in the postischemic kidney. We are compelled to point out that our conclusion of minimal renal endothelial cell proliferation is based on studies using immunohistochemical labeling of endothelial cells with CD31. Although we are unaware of changes in CD31 expression in endothelial cells undergoing proliferation, it is important to

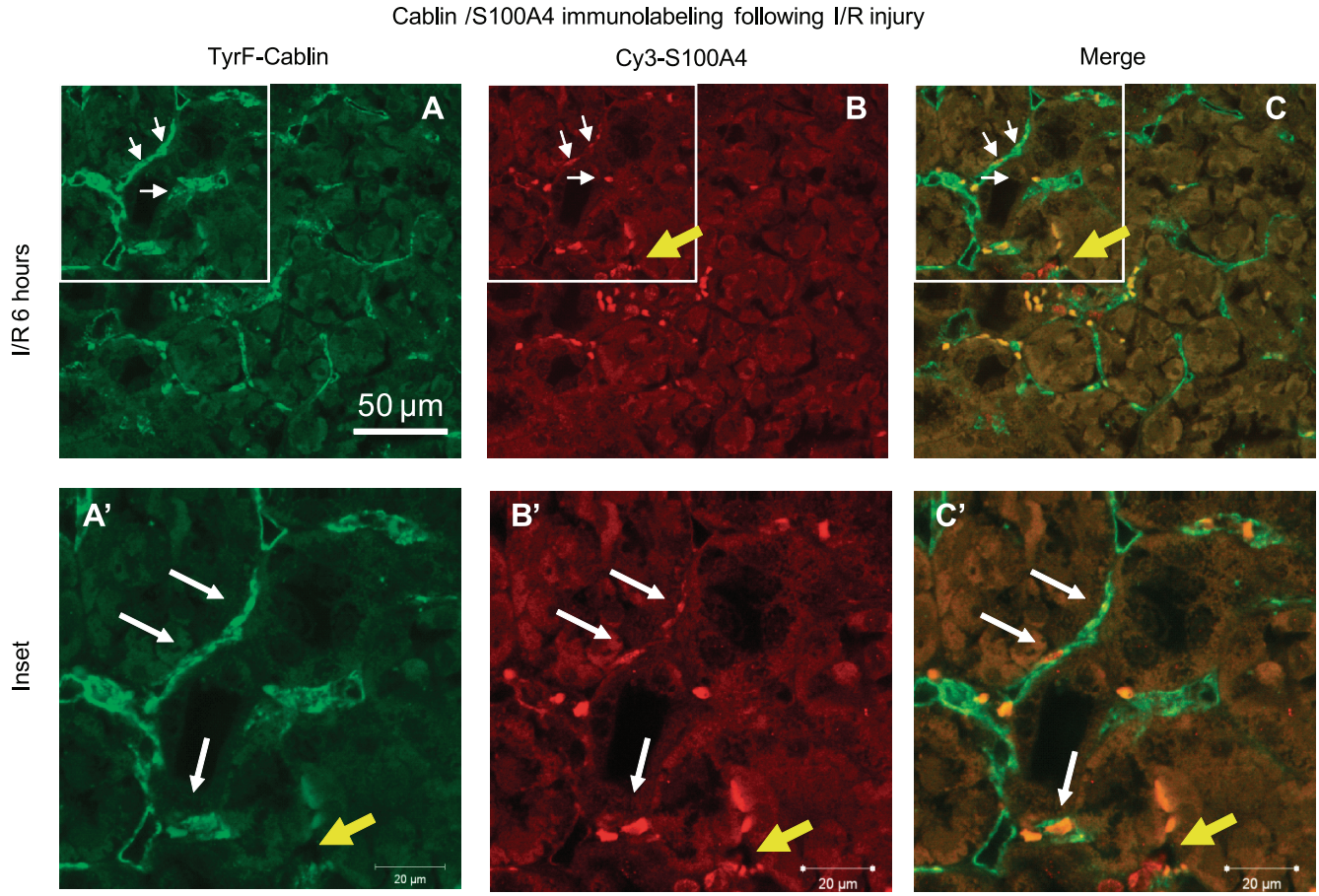

Fig. 8. Colocalization of cablin and S100A4 immunofluorescence following I/R injury. Representative confocal images are shown from kidney of a rat 6 h following renal I/R injury (*A*, *B*, and *C*) and enlarged image of the indicated area are shown in *A′*, *B′*, and *C′*. Cablin staining was achieved by tyramide amplification of fluorescein (*A*, *A′*), while S100A4 was visualized directly using Cy3-labeled secondary (*B*, *B′* see METHODS), while merged images are shown in *C* and *C′*. Magnification is shown in *A*. White arrow indicates double-positive cells, while yellow arrows indicate S100A4-positive/cablin-negative cells. Negative controls (not shown) are similar to Fig. 7. Staining representative of 5 animals per group.

recognize that a transient reduction in CD31 following endothelial cell proliferation would lead us to underestimate the degree of endothelial proliferation.

The mechanism of vascular dropout and the means by which VEGF may protect against it remain unclear. Because the steady state of vascular stability can be recognized as a balance between factors that promote vascular regeneration and vascular loss, it is important to examine both endothelial proliferation as well as possible mechanisms of vascular loss and determine the effects of VEGF-121 on both of these processes. VEGF-121 has been shown to inhibit endothelial apoptosis in human umbilical vein endothelial cells and in glomerular and interstitial cells in a model of thrombotic microangiopathy (40). Therefore, it is possible that the preservation of vascular density post-I/R by VEGF may be due to inhibition of apoptosis. However, in previous studies, we were unable to consistently identify apoptotic cell death following I/R injury (12). Nevertheless, because TUNEL-positive structures are considered to be very transient, it is possible that we may have missed a wave of endothelial apoptosis following injury. Alternatively, the rate of postischemic apoptosis may have been too low to appreciate, but over a long duration may have profound effects. Therefore, we cannot rule out the suggestion that some of the preservation of the renal vasculature are to due to the inhibition of apoptosis by VEGF.

Because our previous studies were not able to identify endothelial apoptosis following I/R, we sought to determine whether phenotypic transition to a mesenchymal cell type represented an alternative mechanism of vascular dropout post-ischemia. The suggestion that endoMT may occur in kidney is supported by recent studies by O'Riordan et al. (30), who demonstrated that NOS inhibition of cultured endothelial cells stimulates differentiation to a myofibroblastic phenotype in vitro. In addition, nonpressor, chronic NOS inhibition in vivo increased cells expressing both endothelial and mesenchymal markers in kidney, indicative of a potential transition state (30).

In the current study, endoMT transitions were identified by colocalization of the fibroblast marker, FSP-1/S100A4, with three different endothelial labeling techniques: *1*) administration of biotinylated tomato lectin, *2*) CD31/PECAM, and *3*) cablin. All of these demonstrated the presence of transition states in the early post-IR period. In contrast to the limited presence of apoptotic endothelial cells (12), endoMT transition states were common within 6 h and sustained for up to 7 days following recovery from I/R. FSP1/S100A4-positive cells were identified in relatively few tubular epithelial cells, suggesting

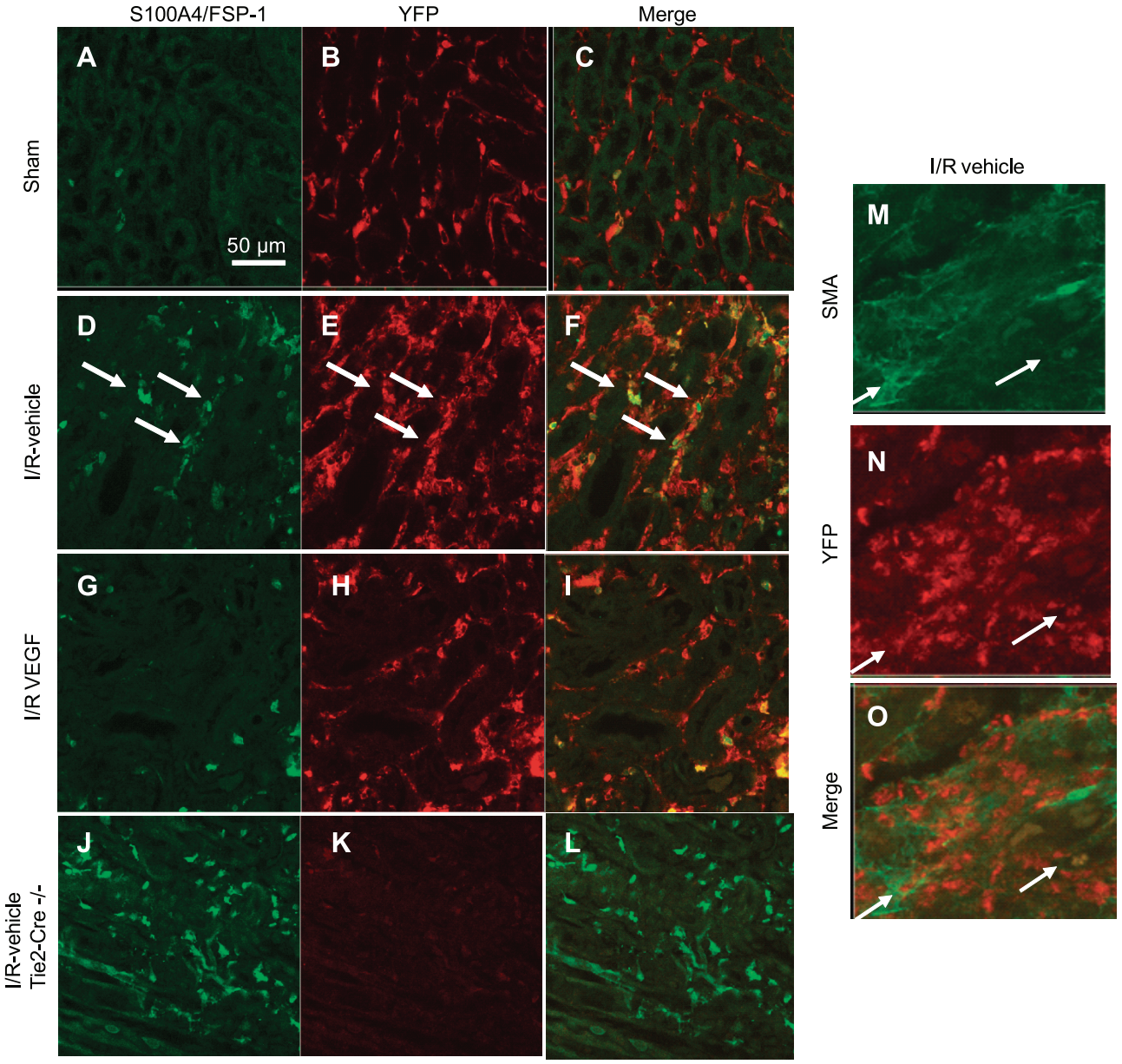

Fig. 9. Effect of renal I/R and recovery on the yellow fluorescent protein (YFP) expression and colocalization with S100A4 and α-smooth muscle actin (SMA) in kidney of Tie2Cre$^{+/-}$YFP$^{+/-}$ mice. Representative confocal images are shown from transgenic Tie2Cre$^{+/-}$YFP$^{+/-}$ mice 14 days following recovery from sham operation (*A*, *B*, *C*) following renal I/R injury (*D*, *E*, and *F*) and following I/R injury with administration of VEGF-121 during the recovery period (*G*, *H*, *I*). Immunofluorescence of S100A4/FSP-1 is shown by fluorescein (*A*, *D*, *G*), YFP expression is shown by Cy3-enhanced immunofluorescence (*B*, *E*, *H*), and respective merged images are shown in *C*, *F*, and *I*. Colocalization of S100A4 cells with YFP is indicated by the white arrows in *D*, *E*, and *F*. Control immunofluorescence was carried out parallel for S100A4 and YFP in post-AKI tissues from Tie2Cre$^{-/-}$YFP$^{+/-}$ mice (*J*, *K*, *L*), in which no signal was observed for YFP (*K*). Similar studies were carried out to localize α-SMA and YFP; representative images are shown for I/R vehicle-treated mice (*M*, *N*, *O*). Arrows indicate cells with staining for both α-SMA and YFP. Magnification is shown in *A*.

that tubular epithelial/mesenchymal transition is a much rarer event than endoMT in the postischemic kidney.

One concern raised by these studies relates to the use of FSP-1/S100A4 as a marker of fibroblasts. There is no widespread consensus regarding a fibroblast-specific marker and although FSP-1/S100A4 also labels macrophages (36), it remains widely utilized for identification of renal interstitial fibroblasts (39). The antibody used in this study clearly labels cells with macrophage morphology. One could argue that endothelial progenitor cells of hematopoietic origin, referred to as an angiogenic macrophages (44), may express both CD31 and FSP-1/S100A4 and that the identification of such cells represents an infiltration rather than a transition following injury. However, FSP-1/S100A4 cells with macrophage morphology do not colocalize with tomato lectin (see Fig. 6). S100A4 is also expressed in certain malignant tumors associated migration and metastasis (16) and also in a variety of injured tissues including arterial smooth muscle cells following stent injury (6). Thus, S100A4 expression may represent a state of cell activation during tissue remodeling.

In addition to identifying potential transition states, we utilized a Cre-Lox transgenic approach to trace the fate of

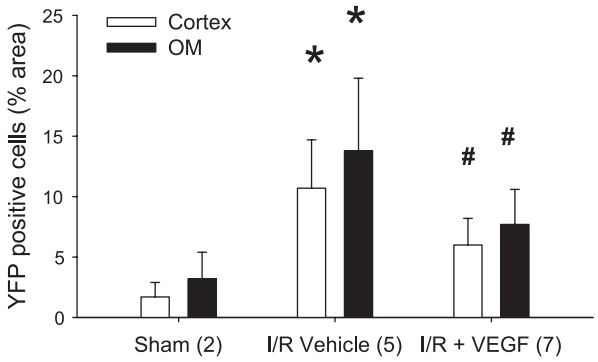

Fig. 10. Effect of AKI and VEGF-121 on the renal interstitial distribution of YFP+ cells from transgenic Tie2Cre$^{+/-}$YFP$^{+/-}$ mice. Data are shown from the renal cortex (open bars) and the renal outer medulla (filled bars) and are expressed as means ± SE. % surface area of YFP+ immunofluorescence was derived from morphometric analysis (see METHODS). The *n* for each group is indicated in the parentheses; *$P < 0.05$ from sham-operated controls; #$P < 0.05$ VEGF-121-treated vs. vehicle-treated post-AKI, based on ANOVA and Student-Newman-Keuls post hoc test.

endothelial cells following injury. This approach is similar to that used by Iwano et al. (15), who labeled tubular epithelial cells and demonstrated that a significant number of interstitial fibroblasts are from epithelial origin in response to unilateral ureteral obstruction, supporting epithelial mesenchymal transition in this model. Recently, Zeisberg et al. (46), used a transgenic approach similar to the one employed in the current study and demonstrated that a significant number of interstitial fibroblasts/myofibroblasts derive from the endothelium in three different models of interstitial fibrosis; i.e., unilateral ureteral obstructive nephropathy, streptozotocin-induced diabetic nephropathy, and a model of Alport renal disease.

The demonstration that YFP-positive S100A4 and α-SMA cells are present in the renal interstitium 14 days after I/R is consistent with the suggestion that a substantial proportion of fibroblasts derives from endoMT in this model. However, it is clear that circulating cells also contribute to a portion of fibroblasts in the postischemic kidney (7, 21). It is worth noting that a Cre-Lox strategy similar to that used to demonstrate epithelial/mesenchymal transition in fibrosis of the unilateral ureteral obstruction (UUO) model has been applied to I/R. In these studies, tubular epithelial cells were shown to dedifferentiate and proliferate following I/R injury, but cells of tubular lineage were not identified in the interstitium (21). These results are consistent with our colocalization data indicating that tubular epithelial transition is not a prominent source of fibroblasts in the I/R model. Finally, the conclusion that interstitial cells derive from endothelial cells relates substantively to the fidelity of the Tie-2/Cre promoter in these transgenic animals; although Tie-2 is a well-accepted marker of endothelial cells, activated pericytes may also express Tie-2. Induced Tie-2 expression in pericytes in response to renal injury would activate YFP expression in these cells and their progeny. Given recent studies by Lin et al. (22), suggesting a prominent role for pericytes in fibrosis following UUO, we cannot be certain that our current studies do not reflect a possible contribution of fibroblasts by pericytes.

Regardless of the etiology of fibroblasts, endoMT could account for the reduction in the number of peritubular blood vessels in the postinjured kidney. Previous studies utilized microvascular filling techniques (4) or endothelial cell staining to measure vascular loss (12, 19). The use endothelial Cre-lox YFP transgenic mice enabled the simultaneous visualization of perfusion through labeled structures in normal and postrecovery kidneys. YFP-positive cells were observed bordering blood vessels identified with dextran perfusion in sham-operated animals. However, the relationship between perfusion and YFP-labeled cells was altered following AKI as multiple YFP-positive cells with differing morphology were present in interstitial areas with either impaired or no blood flow. These results are consistent with the suggestion that endoMT is a primary mechanism of vascular dropout following injury.

Because VEGF-121 appears not to induce proliferation of endothelial cells, while providing protection from vascular loss, it seems reasonable to suggest that VEGF may inhibit endoMT process. This suggestion is supported by our observation that VEGF treatment mitigates, but did not abolish, the interstitial expansion of YFP-positive cells following AKI. To place these results in context, irreversible blood vessel loss in the kidney following IR results from at least two characteristics of the renal endothelial cells. First, renal endothelial cells are predisposed to undergo endoMT in response injury, a process that is at least partially inhibited by VEGF and corresponds to a time at which renal VEGF expression is transiently reduced

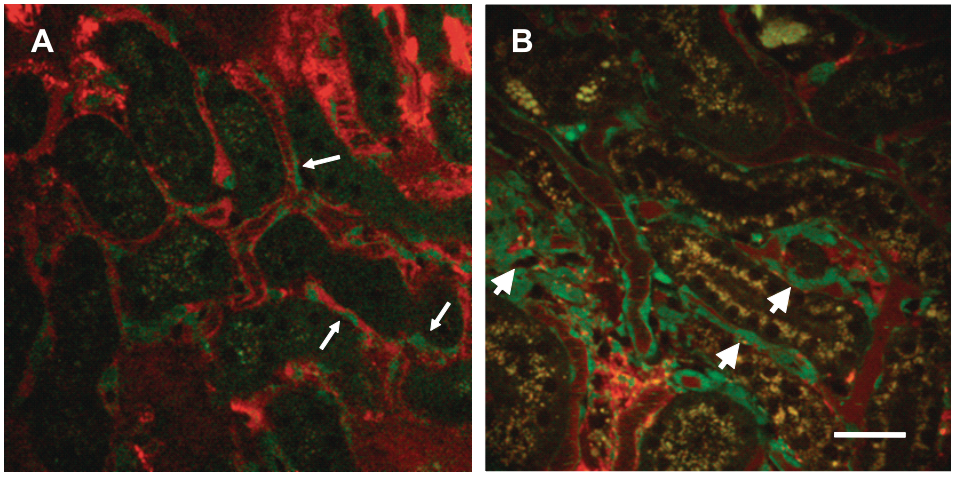

Fig. 11. Effect of renal I/R and recovery on peritubular vascular structure and flow in kidney of Tie2Cre$^{+/-}$YFP$^{+/-}$ mice. Multiphoton images of Tie2Cre$^{+/-}$YFP$^{+/-}$ mouse kidneys were obtained through a lateral flank incision from anesthetized animals 14 days after sham or renal I/R and following the intravenous injection of rhodamine-labeled dextran (MW 500,000). *A*: patent microvessels containing labeled dextran (red) can be observed and bordered by endothelial cells containing YFP, displayed in pseudocolor as green (thin white arrow). Evidence of flow through these vessels is apparent (see supplemental movie). *B*: relatively larger cells are observed in the tubular interstitium expressing YFP (green). These cells are found in areas of reduced or absent flow (indicated by thick arrowhead, see supplemental movie). Bar = 25 μm.

(5). Second, renal endothelial cells have little capacity to proliferate following injury, even in response to exogenous VEGF-121. This is likely the reason for the limited window of time by which VEGF is an effective treatment, such that vascular cells cannot participate in vascular regeneration following the transition to a fibroblastic/myofibroblastic state. This is also consistent with the lack of vascular regeneration following the restoration of VEGF expression following recovery from I/R.

It should be noted that the VEGF-121 used in this study may or may not be a less potent endothelial mitogen than VEGF-165 (26). Therefore, we cannot exclude the possibility that VEGF165 may indeed promote endothelial cell proliferation in this setting. However, we chose to use the nonheparin-binding VEGF-121, because it is easily administered to experimental animals. Following subcutaneous injection, it can be found for several hours in the plasma (40) and targets ischemic tissues (24). In contrast, administration of VEGF-165 is not readily detectable in the plasma following injection (40). In addition, VEGF-121 has been shown to have beneficial effects in other models of kidney disease, including our own study using the model described here (19).

Although the role of hypoxia has received considerable attention as a mediator of progressive disease, not only in AKI but in many settings, its underlying basis relates in part to impaired vascular remodeling processes. It seems reasonable to suggest impaired remodeling may be due to innate characteristics of renal endothelial regarding low proliferative capacity and a predisposition to transdifferentiate. It is currently unknown why renal endothelial cells appear to lack adequate proliferative potential. However, it is clear that not all endothelial cells from all vascular beds have similar growth potentials. Interestingly, Li et al. (20) demonstrated that a smaller proportion of primary endothelial cells from kidney expresses the flk1/KDR/VEGFR2 receptor when compared with endothelial cells from the brain, heart, lung, or liver. These data would be consistent with lower proliferative potential of renal endothelial cells and emphasize the idea that more information is required about endothelial cells from specific vascular beds to understand their normal endogenous growth potential. Future studies may help to determine whether renal endothelial cells can be induced to proliferate by other agents or whether endothelial progenitor cells can be utilized as a substitute to reestablished new blood vessel formation following kidney injury.

GRANTS

This work was supported by National Institutes of Health Grants DK-063114 (to D. Basile), DK-77124 and DK-79312 (to T. Sutton), and DK-069408 (to B. Molitoris) and a George M. O'Brien Grant P30-DK-79312. Support for J. Friedrich was provided by the Undergraduate Research Opportunity Program at Indiana University Purdue University Indianapolis, and support for J. Spahic was provided by Indiana University Life Health Science Internship program.

Present address of S. Changizi-Ashtiyani: Dept. of Physiology, Arak Univ. of Medical Sciences, Arak, Iran.

DISCLOSURES

No conflicts of interest, financial or otherwise, are declared by the author(s).

REFERENCES

1. **Askenazi D, Feig D, Graham N, Hui-Stickle S, Goldstein SL.** 3–5 Year longitudinal follow-up of pediatric patients after acute renal failure. *Kidney Int* 69: 184–189, 2006.
2. **Basile DP.** The endothelial cell in ischemic acute kidney injury: implications for acute and chronic function. *Kidney Int* 72: 151–156, 2007.
3. **Basile DP, Donohoe DL, Roethe K, Mattson DL.** Chronic renal hypoxia following ischemia/reperfusion injury: effects of L-arginine on hypoxia and secondary damage. *Am J Physiol Renal Physiol* 284: F338–F348, 2003.
4. **Basile DP, Donohoe DL, Roethe K, Osborn JL.** Renal ischemic injury results in permanent damage to peritubular capillaries and influences long-term function. *Am J Physiol Renal Physiol* 281: F887–F899, 2001.
5. **Basile DP, Fredrich K, Chelladurai B, Leonard EC, Parrish AR.** Renal ischemia reperfusion inhibits VEGF expression and induces ADAMTS-1, a novel VEGF inhibitor. *Am J Physiol Renal Physiol* 294: F928–F936, 2008.
6. **Brisset AC, Hao H, Camenzind E, Bacchetta M, Geinoz A, Sanchez JC, Chaponnier C, Gabbiani G, Bochaton-Piallat ML.** Intimal smooth muscle cells of porcine and human coronary artery express S100A4, a marker of the rhomboid phenotype in vitro. *Circ Res* 100: 1055–1062, 2007.
7. **Broekema M, Harmsen MC, van Luyn M, Koerts J, Persersen AH, Kooten TG, van Goor H, Navis G, Popa ER.** Bone marrow-derived myofibroblasts contribute to renal interstital myofibroblasts population and produce procollagen I after ischemia reperfusion in rats. *J Am Soc Nephrol* 18: 165–175, 2007.
8. **Charron AJ, Xu W, Bacallao RL, Wandinger-Ness A.** Cablin: a novel protein of the capillary basal lamina. *Am J Physiol Heart Circ Physiol* 277: H1985–H1996, 1999.
9. **Chevalier RL, Forbes MS, Thornhill BA.** Ureteral obstruction as a model of renal interstitial fibrosis and obstructive nephropathy. *Kidney Int* 75: 1145–1152, 2009.
10. **Coca SG.** Acute kidney injury in elderly persons. *Am J Kidney Dis* 56: 122–131, 2010.
11. **Coca SG, Yusuf B, Shlipak MG, Garg AX, Parikh CR.** Long-term risk of mortality and other adverse outcomes after acute kidney injury: a systematic review and meta-analysis. *Am J Kidney Dis* 53: 961–973, 2009.
12. **Horbelt M, Lee SY, Mang HE, Knipe NL, Sado Y, Kribben A, Sutton TA.** Acute and chronic microvascular alterations in a mouse model of ischemic acute kidney injury. *Am J Physiol Renal Physiol* 293: F688–F695, 2007.
13. **Humes D, Cieslinski DA, Coimbra TM, Messana JM, Galvao C.** Epidermal growth factor enhaces renal tubule cell regeneration and repair and accelerates the recovery of renal function in postischemic acute renal failure. *J Clin Invest* 84: 1757–1761, 1989.
14. **Ishani A, Xue JL, Himmelfarb J, Eggers PW, Kimmel PL, Molitoris BA, Collins AJ.** Acute kidney injury increases risk of ESRD among elderly. *J Am Soc Nephrol* 20: 223–228, 2009.
15. **Iwano M, Plieth D, Danoff TM, Xue C, Okada H, Neilson EG.** Evidence that fibroblasts derive from epithelium during tissue fibrosis. *J Clin Invest* 110: 341–350, 2002.
16. **Jenkinson SR, Barraclough R, West CR, Rudland PS.** S100A4 regulates cell motility and invasion in an in vitro model for breast cancer metastasis. *Br J Cancer* 90: 253–262, 2004.
17. **Johnson RJ, Schreiner GF.** Hypothesis: the role of acquired tubulointerstitial disease in the pathogenesis of salt-dependent hypertension. *Kidney Int* 52: 1169–1179, 1997.
18. **Kang DH, Anderson S, Kim YG, Mazzalli M, Suga S, Jefferson JA, Gordon KL, Oyama TT, Hughes J, Hugo C, Kerjaschki D, Schreiner GF, Johnson RJ.** Impaired angiogenesis in the aging kidney: vascular endothelial growth factor and thrombospondin-1 in renal disease. *Am J Kidney Dis* 37: 601–611, 2001.
19. **Leonard EC, Friderich J, Basile DP.** VEGF-121 preserves renal microvessel structure and ameliorates secondary renal disease following acute kidney injury. *Am J Physiol Renal Physiol* 295: F1648–F1657, 2008.
20. **Li W, Johnson S, Shelley W, Yoder M.** Hematopoietic stem cell repopulating ability can be maintained in vitro by some primary endothelial cells. *Exp Hematol* 32: 1226–1237, 2004.
21. **Lin F, Moran A, Igarashi P.** Intrarenal cells, not bone marrow-derived cells are the major source of regeneration of the postischemic kidney. *J Clin Invest* 115: 1756–1764, 2005.

22. **Lin SL, Kisseleva T, Brenner DA, Duffield JS.** Pericytes and perivascular fibroblasts are the primary source of collagen-producing cells in obstructive fibrosis of the kidney. *Am J Pathol* 173: 1617–1627, 2008.
23. **Long D, Mu W, Price K, Roncal C, Schreiner GF, Woolf AS, Johnson R.** Vascular endothelial growth factor administration does not improve microvascular disease in the salt-dependent phase of postangiotensin II hypertension. *Am J Physiol Renal Physiol* 291: F1248–F1254, 2006.
24. **Lu E, Wagner WR, Schellenberger U, Abraham JA, Klibanov AL, Woulfe SR, Csikari MM, Fischer D, Schreiner GF, Brandenburger GH, Villanueva FS.** Targeted in vivo labeling of receptors for vascular endothelial growth factor: approach to identification of ischemic tissue. *Circulation* 108: 97–103, 2003.
25. **Miller SB, Martin DR, Kissane J, Hammerman MR.** Insulin-like growth factor I accelerates recovery from ischemic acute tubular necrosis in the rat. *Proc Natl Acad Sci USA* 89: 11876–11880, 1992.
26. **Neufeld G, Cohen T, Gengrinovitch S, Poltorak Z.** Vascular endothelial growth factor (VEGF) and its receptors. *FASEB J* 13: 9–22, 1999.
27. **Nigam SK, Lieberthal W.** Acute renal failure. III. The role of growth factors in the process of renal regeneration and repair. *Am J Physiol Renal Physiol* 279: F3–F11, 2000.
28. **Nony PA, Schnellmann RG.** Mechanisms of renal cell repair and regeneration after acute renal failure. *J Pharmacol Exp Ther* 304: 905–912, 2003.
29. **Ojo AO, Hanson JA, Wolfe RA, Leichtman AB, Agodoa LY, Port FK.** Long-term survival in renal transplant recipients with graft function. *Kidney Int* 57: 307–313, 2000.
30. **O'Riordan E, Mendelev N, Patschan S, Patschan D, Eskander J, Cohen-Gould L, Chander P, Goligorsky MS.** Chronic NOS inhibition actuates endothelial-mesenchymal transformation. *Am J Physiol Heart Circ Physiol* 292: H285–H294, 2007.
31. **Ostendorf T, Kunter U, Eitner F, Loos A, Regele H, Kerjaschki D, Henninger DD, Janjic N, Floege Jr.** VEGF165 mediates glomerular endothelial repair. *J Clin Invest* 104: 913–923, 1999.
32. **Padanilam BJ.** Cell death induced by acute renal injury: a perspective on the contributions of apoptosis and necrosis. *Am J Physiol Renal Physiol* 284: F608–F627, 2003.
33. **Pechman KR, De Miguel C, Lund H, Leonard EC, Basile DP, Mattson DL.** Recovery from renal ischemia-reperfusion injury is associated with altered renal hemodynamics, blunted pressure natriuresis, and sodium-sensitive hypertension. *Am J Physiol Regul Integr Comp Physiol* 297: R1358–R1363, 2009.
34. **Ray PE, Suga S, Liu XH, Huang X, Johnson RJ.** Chronic potassium depletion induces renal injury, salt sensitivity, and hypertension in young rats. *Kidney Int* 59: 1850–1858, 2001.
35. **Schmitt R, Cantley LG.** The impact of aging on kidney repair. *Am J Physiol Renal Physiol* 294: F1265–F1272, 2008.
36. **Schneider M, Kostin S, Strøm CC, Aplin M, Lyngbaek S, Theilade J, Grigorian M, Andersen CB, Lukanidin E, Lerche Hansen J, Sheikh SP.** S100A4 is upregulated in injured myocardium and promotes growth and survival of cardiac myocytes. *Cardiovasc Res* 75: 40–50, 2007.
37. **Spurgeon-Pechman KR, Donohoe DL, Mattson DL, Lund H, James L, Basile DP.** Recovery from acute renal failure predisposes hypertension and secondary renal disease in response to elevated sodium. *Am J Physiol Renal Physiol* 293: F269–F278, 2007.
38. **Spurgeon KS, Donohoe DL, Basile DP.** Transforming growth factor-β in acute renal failure: receptor expression, influence in cell proliferation, cellularity and vascularization after recovery from injury. *Am J Physiol Renal Physiol* 288: F568–F577, 2005.
39. **Strutz F, Zeisberg M.** Renal fibroblasts and myofibroblasts in chronic kidney disease. *J Am Soc Nephrol* 17: 2992–2998, 2006.
40. **Suga S, Kim YG, Joly A, Puchacz E, Kang DH, Jefferson JA, Abraham JA, Hughes J, Johnson RJ, Schreiner GF.** Vascular endothelial growth factor (VEGF121) protects rats from renal infarction in thrombotic microangiopathy. *Kidney Int* 60: 1297–1308, 2001.
41. **Witzenbichler B, Asahara T, Murohara T, Silver M, Spyridopoulos I, Magner M, Principe N, Kearney M, Hu JS, Isner JM.** Vascular endothelial growth factor-C (VEGF-C/VEGF-2) promotes angiogenesis in the setting of tissue ischemia. *Am J Pathol* 153: 381–394, 1998.
42. **Xu B, Wu YQ, Huey M, Arthur HM, Marchuk DA, Hashimoto T, Young WL, Yang GY.** Vascular endothelial growth factor induces abnormal microvasculature in the endoglin heterozygous mouse brain. *J Cereb Blood Flow Metab* 24: 237–244, 2004.
43. **Xue JL, Daniels F, Star RA, Kimmel PL, Eggers PW, Molitoris BA, Himmelfarb J, Collins AJ.** Incidence and mortality of acute renal failure in medicare beneficiaries, 1992 to 2001. *J Am Soc Nephrol* 17: 1135–1142, 2006.
44. **Yoder MC, Mead LE, Prater D, Krier TR, Mroueh KN, Li F, Krasich R, Temm CJ, Prchal JT, Ingram DA.** Redefining endothelial progenitor cells via clonal analysis and hematopoietic stem/progenitor cell principals. *Blood* 109: 1801–1809, 2007.
45. **Yuan HT, Li XZ, Pitera JE, Long DA, Woolf AS.** Peritubular capillary loss after mouse acute nephrotoxicity correlates with downregulation of vascular endothelial growth factor-A and hypoxia-inducible factor-1 alpha. *Am J Pathol* 163: 2289–2301, 2003.
46. **Zeisberg EM, Potenta SE, Sugimoto H, Zeisberg M, Kalluri R.** Fibroblasts in kidney fibrosis emerge via endothelial-to-mesenchymal transition. *J Am Soc Nephrol* 19: 2282–2287, 2008.